ELSEVIER

PHYSICA A

Spatial distribution of avalanches in invasion percolation: their role in fingering

M. Ferer[a,b,*], Grant S. Bromhal[c], Duane H. Smith[c,b]

[a] *National Energy Technology Laboratory, Morgantown, WV 26507-0880, USA*
[b] *Department of Physics, West Virginia University, Morgantown, WV 26506-6315, USA*
[c] *US DOE, National Energy Technology Laboratory, Morgantown, WV 26507-0880, USA*

Received 5 March 2002

Abstract

For two decades, invasion percolation (IP) has provided a simple model of 'drainage' where a non-wetting fluid is injected into a porous media saturated with a wetting fluid, in the limit where capillary forces dominate and viscous forces are negligible. IP produces a characteristic fingering with a fractal dimension close to that of ordinary critical percolation. Avalanches (also called 'bursts' or 'Haines jumps') have been observed. In this paper, we focus on the practical issues relating to the causes of the fingering and of the low saturations of injected fluid. We show that the saturation and the average position of the injected fluid exhibit standard fractal scaling behavior. However, the fractional flow of the injected fluid does not allow an average analysis because of the noise arising from the avalanches, even for the million site systems investigated in this paper. In studying the spatial distribution of these avalanches, we find a size cutoff depending upon the position of the avalanches; this is characteristic of the finite size of the system and signals that the systems have not achieved self-organized criticality. Furthermore, we show that the average size of these avalanches, $\langle s_a \rangle$, increases with their average distance, $\langle x \rangle$, from the outlet as $\langle s_a \rangle \approx \langle x \rangle^{1.1}$. As a result, larger avalanches will tend to occur at the end of longer fingers causing preferential growth of the long fingers at the expense of the shorter fingers.

PACS: 47.55.Mh; 47.55.Kf; 64.60.Ak

Keywords: Invasion percolation; Flow in porous media; Depinning transitions; Self-organized criticality

* Corresponding author. National Energy Technology Laboratory, Morgantown, WV 26507-0880, USA.
E-mail address: martin.ferer@or.netl.doe.gov (M. Ferer).

1. Introduction

The fingering of the injected fluid associated with immiscible, two-phase flow in porous media is one of the major reasons why several important geologic recovery/remediation processes are singularly inefficient. In secondary oil recovery, the water displaces much less than half of the oil in any given reservoir, because the water 'fingers' into the oil-saturated reservoir. In CO_2 sequestration, where greenhouse gases are injected into water saturated porous media (sea floor, deep water table, etc.) for purposes of storage, the percent of possible storage is limited by the fingering of CO_2 into reservoir so that only a small fraction of the reservoir is occupied by CO_2. In remediation of DNAPL or LNAPL spills, which have entered and contaminated the water table, standard pump and treat remediation methods are extremely inefficient because the water used to flush the contaminant from the porous media does not mobilize the pollutant and only removes that tiny percentage which will be dissolved in the water. Because of our focus on the efficiency of these processes, it is important to understand how the injected fluid occupies the medium. Therefore, this study investigates the average position and saturation of the non-wetting, injected fluid, when the reservoir is saturated by a wetting fluid.

For decades, it has been appreciated that these processes are least efficient at low injection rates, i.e., at small capillary numbers, $N_c = (\text{viscous forces})/(\text{capillary forces})$, where the capillary forces dominate [1]. In the extreme limit of infinitesimal injection rate, effectively zero capillary number, Wilkinson and others introduced a simple model of immiscible, two-phase flow called invasion percolation (IP) [2,3]. In this model, the non-wetting, injected fluid only advances through the largest throat (the one with the smallest capillary pressure) on the interface between the injected, non-wetting fluid and the wetting, defending fluid.

This IP model has been widely studied since its introduction [2–8]. The injection patterns have been shown to be self-similar fractals with a fractal dimension similar to that from standard percolation processes; recent work suggests that they may be identical [2–8]. It has been argued that this simplest version, just described, is inadequate in two dimensions, where a region of wetting fluid can be 'trapped' if the non-wetting, injected fluid flows around the region of wetting fluid, fully encircling it and, thereby blocking its route to the outlet of the porous medium [3]. A number of these 'trapped' regions can be seen near the inlet of the pattern in Fig. 1.

In the limit of zero capillary number, viscous effects are zero, so that the pressures are uniform throughout any one fluid. Therefore, the pressure in the injected fluid is uniformly equal to the inlet pressure while the pressure in the wetting fluid is uniformly equal to the outlet pressure. The pressure drop at the interface (inlet pressure minus outlet pressure) is just large enough to advance the non-wetting fluid through the largest allowed throat on the interface. Therefore, this pressure drop must always be positive and the wetting fluid cannot displace the non-wetting fluid from an occupied pore-body. Since the wetting fluid cannot displace the non-wetting fluid, a fully encircled region of wetting fluid is immobilized or trapped, in that the non-wetting fluid is prevented from advancing into this trapped region. (IP) with trapping (IPwt) modifies the standard IP rules to forbid any advance into a 'trapped' region. Recently, we have presented

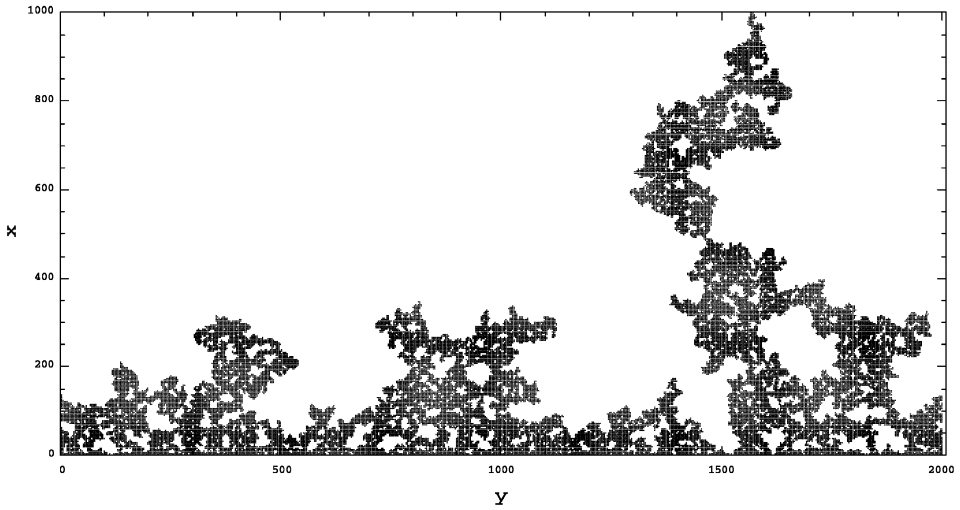

Fig. 1. The injected fluid occupation of a typical million site diamond lattice up to breakthrough.

results from a standard model of two-phase flow in porous media which shows that the model reproduces saturations and flow patterns from IPwt in the limit of small capillary number [9].

The flow in the IPwt exhibits phenomena, variously called 'bursts' or 'Haines jumps' or 'avalanches', where the advance of the interface occurs in a localized region. In this region, capillary pressures are lower than anywhere else on the interface. These avalanches were first studied in sandpile models of self-organized criticality (SOC) [10,11]. These sandpile systems were found to self-organize to a critical point where avalanches of all sizes occurred and where the size distribution of these avalanches obeyed a power law. These avalanches were observed in IPwt [7]; and a scaling theory was developed to describe the number distribution and self-correlation of these avalanches [6].

Unfortunately, this understanding of the IPwt model does not fully explain issues of practical interest, i.e., why the fingering occurs and why the saturation of the injected fluid is so small. To understand better these issues for immiscible injection at small capillary number, we have studied IPwt in two dimensions on a number of realizations of model systems with pore bodies at the sites of a diamond lattice connected by throats of randomly chosen cross-sectional area; we have studied model systems with a variety of sizes up to a size of 10^6 pore bodies (400×2500 and 1000×1000). A typical pattern is shown in Fig. 1. In Section 2, we show that advance of the injected fluid is described by the same fractal dimension describing patterns from standard percolation theory. That is, the time dependence of the first moment of the injected fluid and its saturation are characterized by this fractal dimension. However, in Section 3, when we look at the fractional flow profiles (the position dependence of the flow of the injected fluid, i.e., the current associated with saturation), we do not observe the expected regular advance of the injected fluid through the medium. Instead, we observe

a very noisy interfacial advance associated with the local advance from 'bursts' or 'Haines jumps' or 'avalanches'. In Section 4, we find that these avalanches have the predicted size distribution and correlations. When we look at the spatial distribution of these avalanches, in Section 5, we find convincing evidence that the avalanche size, s_a (i.e., the mass or volume of injected fluid in the avalanche), increases with distance x from the inlet and indeed that the avalanche size shows an almost linear growth with distance from the inlet, $\langle s_a \rangle \approx \langle x \rangle^{1.1}$. If the size of these local avalanches are increasing with x, i.e., with finger length, the long fingers grow at the expense of the shorter fingers; i.e., larger x means larger avalanches and a larger advance of the long fingers.

2. Average position—first moment of the injected fluid

In this section, we investigate the average distance from the inlet, $\langle x \rangle$, of the injected fluid as a function of injected volume, V, equivalently mass, m, or 'time'. For a constant volume flow, q, the volume is directly proportional to the time, $V = qt$, as is the mass of negligibly compressible fluids. An additional advantage of determining the time dependence of $\langle x(t) \rangle$ is its simple relationship to fractal dimension for fractal flows like those from IPwt. Since the mass of a fractal, m, is related to the linear dimension, $\langle x \rangle$, $m = A\langle x \rangle^{D_f - 1}$, then $\langle x(t) \rangle$ is given by

$$\langle x(t) \rangle = Bt^{1/(D_f - 1)} = Bt^{1+\varepsilon}, \quad t = (m/w) + 0.91 \tag{1}$$

which defines the exponent, ε. Fig. 2 shows data from a variety of IPwt simulations from systems with different sizes (from small diamond lattices of length 30 pore bodies and widths from 90 to 270 with a few thousand pore bodies to lattices with one million pore bodies 400×2500). In our definition of 'time' (i) we use the mass (equivalently the volume, both proportional to the physical time), which would enable us to compare the fractal character from computer experiments with different flow velocities; (ii) given our uniform injection along the width of the diamond lattice, we divide the mass by the width because time is unaffected by the width of different model even though the mass would be proportional to that width; (iii) the additive constant of 0.91 arises from the discrete vs. continuous arguments of our earlier miscible flow work [12] (irrelevant at larger times, it serves as a fitting constant to make the power law in Eq. (1) applicable at smaller times) and; (iv) the exponent $1 + \varepsilon = 1.123$ represents the prediction using the known value of the percolation dimension, $D_f = 1.89$. This value of the fractal dimension agrees with later work on IPwt although it is somewhat larger than that found in other studies of IPwt, $D_f = 1.82$ [4–8,13].

We have focused on 'short, wide' systems because experience has shown that flows in long narrow systems (even in square systems) coarsen from many growing fractal fingers to one growing finger [14]. This causes significant deviations from fractal power laws. The values of $\langle x \rangle / t^{1.123}$ exhibit significant noise even for our wide systems and after averaging over as many as 20 different realizations. It seems likely that randomly positioned avalanches, to be discussed in Section 4, are responsible for this significant

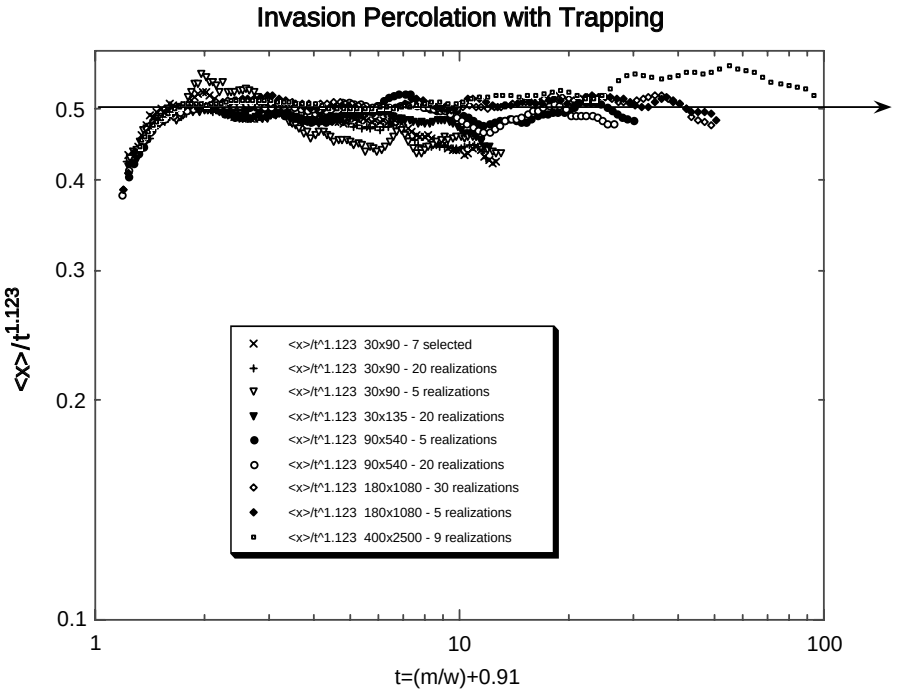

Fig. 2. Fractal scaling of $\langle x(t)\rangle$ from IPwt on a variety of systems sizes averaging over a variety of numbers of realizations (different samples of our model system which differ only in the random number seed used to generate the throat widths).

amount of this noise. Even with the random noise, there are no consistent trends which would make the slope of the data in Fig. 2 significantly different from zero.

3. Saturation profiles for IPwt

We have performed IPwt simulations on five different realizations of systems which are 400 pore bodies in the direction of flow (the x direction) and 2500 pore bodies wide (in the y direction). The following figure shows the results of averaging the saturation profile over five realizations. This saturation profile gives the fraction of the porous medium occupied by the invading fluid at a given value of x for four different times: when 4%, 6%, 10% and 12% of the porous medium is occupied by invading fluid, respectively.

Since the first moment of these profiles is exactly the $\langle x\rangle$ discussed in the previous section, the time dependence of $\langle x\rangle$ makes definite predictions about the time dependence of the saturation profiles. If $\langle x(t)\rangle$ must obey Eq. (1), the saturation profile must have the following 'scaling' form:

$$S(x,t) = t^{-\varepsilon}\zeta(x/t^{1+\varepsilon})\,, \tag{2}$$

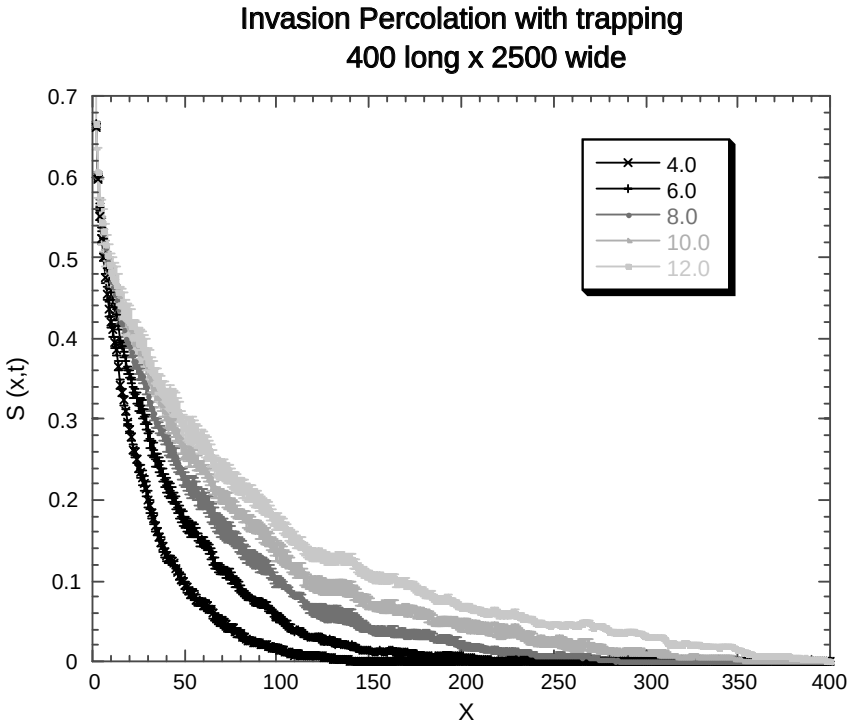

Fig. 3. The saturation profiles (from averaging over five realizations) at times when 4%, 6%, 8%, 10% and 12% of the porous medium is occupied by invading fluid.

where ζ is an undetermined function. Eq. (2) follows because of the following two relations. First, the total saturation is equal to t (in this section, the fraction (or percent) of the porous medium occupied by invading fluid), i.e.,

$$t = \int S(x,t)\,\mathrm{d}x = \int t^{-\varepsilon}\varsigma(x/t^{1+\varepsilon})\,\mathrm{d}x = t\int \varsigma(u)\,\mathrm{d}u\,, \tag{3}$$

where u is the variable $u = x/t^{1+\varepsilon}$, and the last integral is dimensionless. Secondly, the first moment of the saturation profile is just the $\langle x(t)\rangle$ analyzed in the previous sections, which must satisfy Eq. (1) for IP so that

$$\langle x\rangle = \int xS(x,t)\,\mathrm{d}x = \int xt^{-\varepsilon}\varsigma(x/t^{1+\varepsilon})\,\mathrm{d}x = t^{1+\varepsilon}\int u\varsigma(u)\,\mathrm{d}u\,. \tag{4}$$

The scaling form in Eq. (2) is the only function which satisfies these relations for the leading power of t in Eq. (1). (Note: the difference between the definitions of time in this section and the previous one is purely multiplicative length of the system and has no effect upon the power-law dependence in these equations.)

Therefore, we have a definite prediction (Eq. (2)) for the saturation profiles. Fig. 4 tests this prediction for the data in the above figure for the saturation profiles.

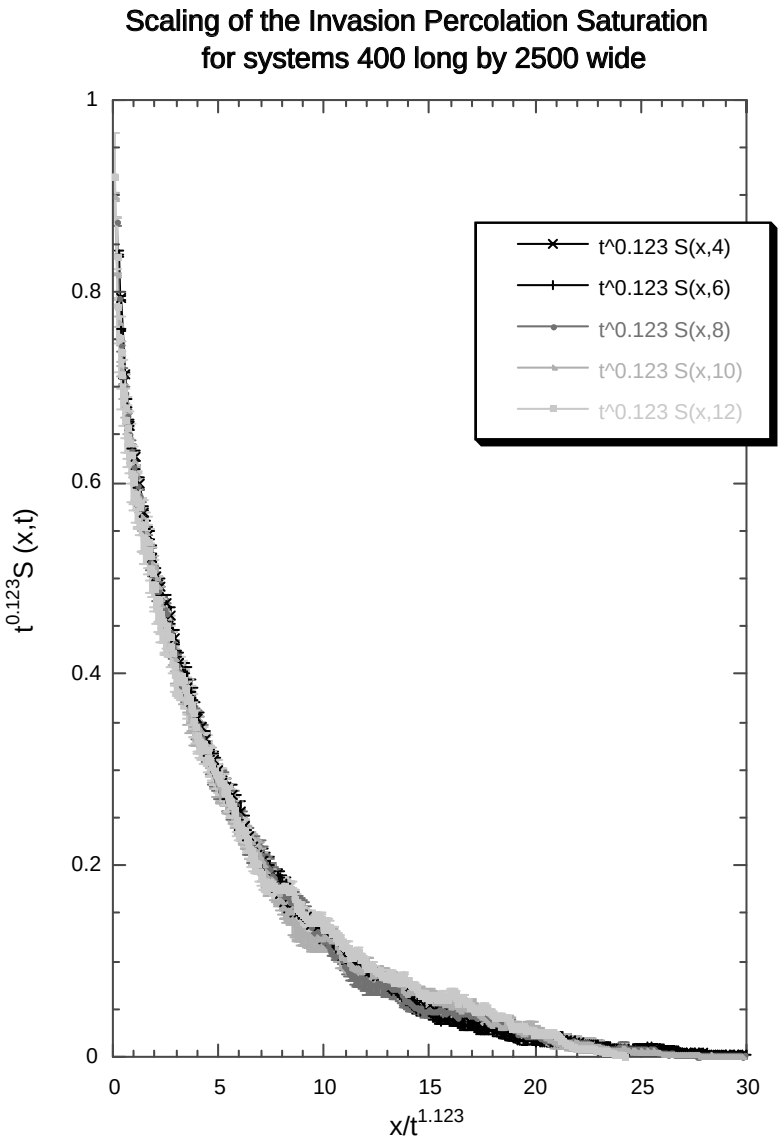

Fig. 4. The scaling form of Eq. (2) as required by the behavior of the first moment (Eq. (1)) for IP.

Since $s(u)$ should equal $t^{\varepsilon}\ S(x,t)$ and should be only a function of $u = x/t^{1+\varepsilon}$, the four curves in Fig. 3 should collapse to the one curve defining the function $\zeta(u)$. To well within the small error bars shown in Fig. 4, the data show striking agreement with the prediction of Eq. (2).

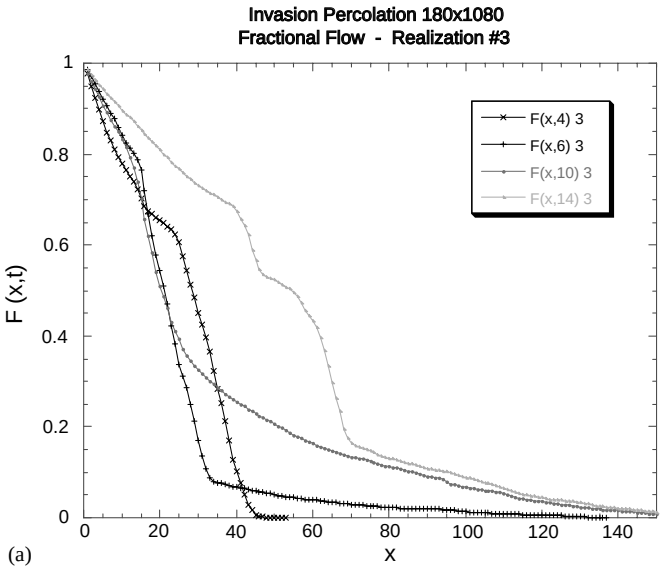

(a)

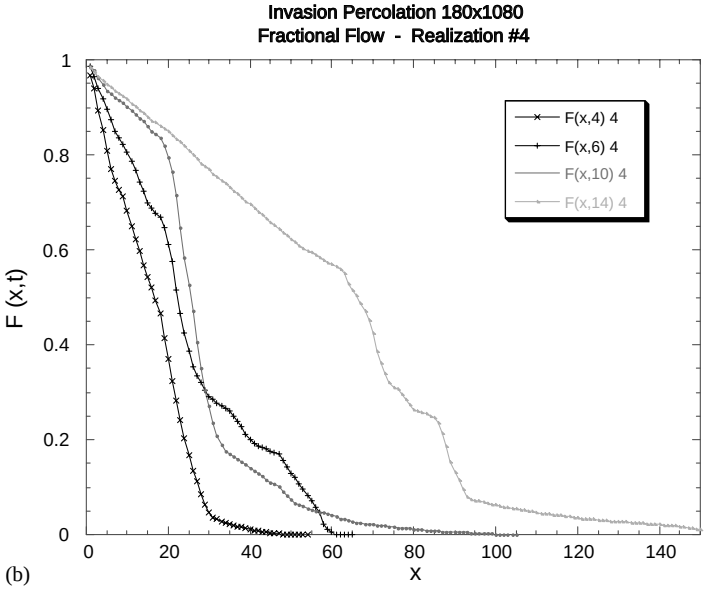

(b)

Fig. 5. (a and b). Fractional flow profiles for two different realizations of the 180×1080 systems.

3.1. Fractional flow profiles

Surprisingly, given the smooth behavior of the saturation profiles, the fractional flow profiles are quite noisy. Figs. 5a, b show the fractional flow profiles at the four times $t = 4\%$, 6%, 10% and 14% for two different, but typical, realizations. In all cases,

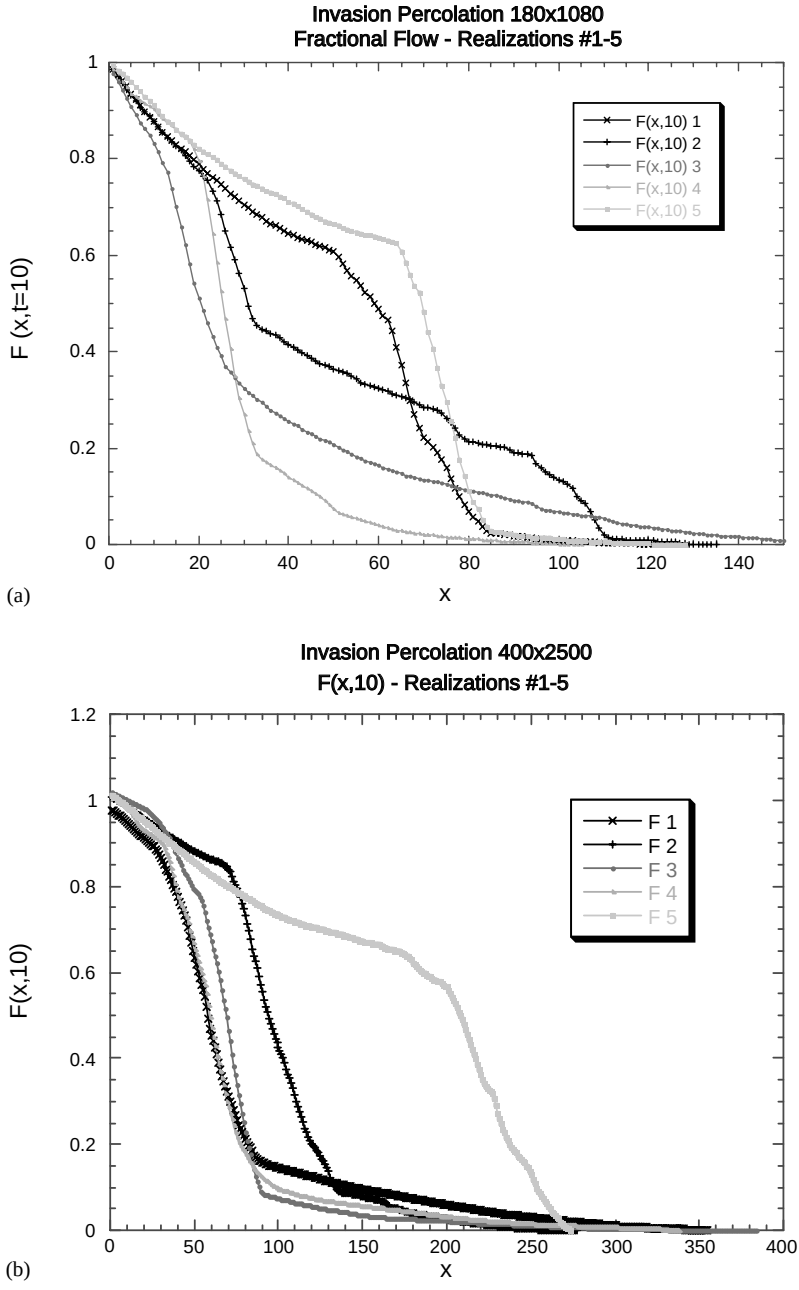

Fig. 6. The fractional flow profiles at $t=10$ for the five different realizations of (a) 180×1080, (b) 400×2500 systems.

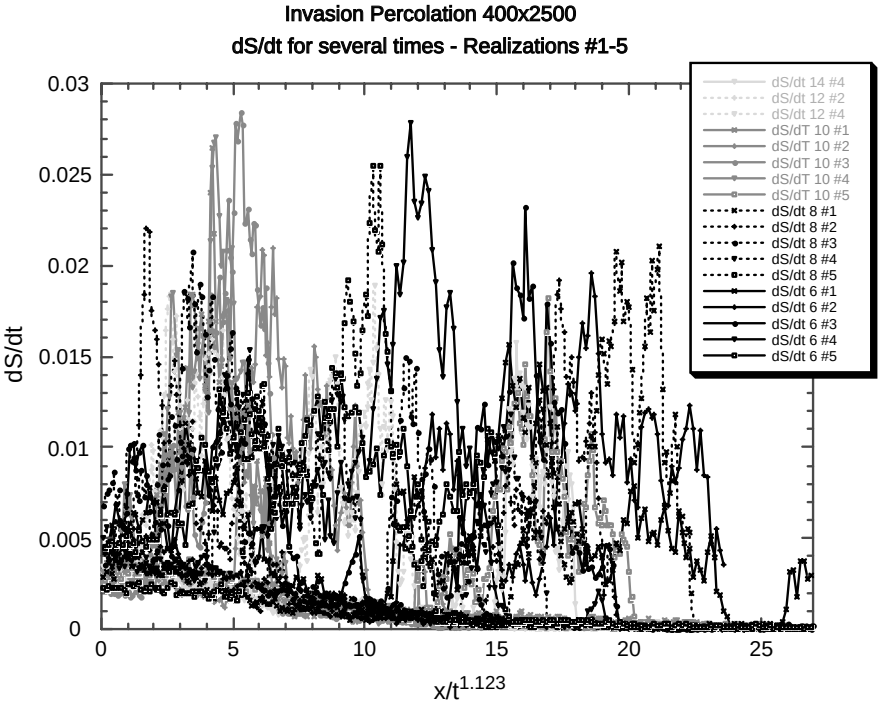

Fig. 7. The effect of the 'bursts' showing the change in saturation at $t = 6\%$, 8%, 10%, 12% and 14% as a function of scaled distance. Only some realizations are represented at $t = 12\%$ and 14% because breakthrough occurred earlier for the other realizations.

these fractional flow profiles are characterized by 'bursts' (or 'avalanches' or 'Haines jumps') where the interface advances rapidly and where the fractional flow changes dramatically. Disconcertingly, these 'bursts' seem to occur at random locations without any regular progression as the invading fluid moves through the medium; also, there are significant differences between realizations (different samples of our model system which differ only in the random number seed used to generate the throat widths). Fig. 6a, b compares the fractional flow profiles for $t = 10$ for five different porous media for the 180×1080 and the 400×2500 size systems, respectively; again, the locations of the 'bursts' seem random, i.e., very sensitive to the differences between the realizations.

Given the nature of the IP model, it is not surprising that the interfacial advance occurs randomly throughout the porous medium, since the fluid only advances into the largest interfacial throat (with the smallest capillary pressure to overcome). Therefore, at any one time step, the interface advances only through that largest interfacial throat, and that largest throat may be anywhere on the interface. Actually, Figs. 5 and 6 should be less noisy than the situation just described, because Figs. 5 and 6 include the interfacial advance not just during one time step but during a short time, dt, where 0.1% of the porous medium has been invaded. That is, the fractional flow at $t = 10\%$ reflects the

change in saturation between $t = 9.9\%$ and 10%; effectively, we have averaged the fractional flow over many time steps (approximately 200 for porous media of the size under consideration). Still, the fractional flow profile is disconcertingly noisy, making analysis of the average behavior difficult if not meaningless. This time-averaged fractional flow shows the 'bursts' which dominate the flow during this 0.1% time interval.

It is easy to appreciate the randomness in the locations and ranges of these bursts if we look at the rate of change of the saturation of injected fluid instead of the fractional flow. Fig. 7 shows $[\mathrm{d}S(x,t)]/\mathrm{d}t|_t$ averaged over times from t-0.1 to t for $t = 6\%$, 8%, 10%, 12% and 14%. In order to compare the burst locations at different times, we have plotted $[\mathrm{d}S(x,t)]/\mathrm{d}t|_t$ vs. the scaled position $x/t^{1.123}$ for the five different realizations.

Since this is the slope of the fractional flow profile, the large slopes in Fig. 6 ('bursts') show up as large values of $[\mathrm{d}S(x,t)]/\mathrm{d}t|_t$. Notice the 'bursts are randomly distributed over the scaled distance; specifically, there are $t = 6\%$ 'bursts' (solid black lines) over the full range of scaled distance, and $t = 8\%$ 'bursts' (dashed black lines) over the full range of scaled distance; the $t = 10\%$ 'bursts' (solid, dark gray lines) are more clustered at small-to-mid-range scaled distance, consistent with Fig. 6b. Clearly, the 'bursts' or avalanches occur randomly at all values of scaled distance.

4. Avalanche ('burst' or 'Haines jump') distributions

For more than a decade, it has been known that avalanches occur in IP and that these avalanches obey scaling relations related to ordinary percolation theory [6,7,13]. The avalanches occur when a throat is invaded and then a series of throats connected to this original seed throat are sequentially invaded; this occurs because the seed throat is the inlet to a region in the lattice with comparatively small capillary pressures [6]. The mass-distribution of avalanches was predicted to be a power law function of size

$$N \propto s_{\mathrm{a}}^{\tau'}, \tag{5}$$

again s_{a} is the size (mass) of an avalanche. The exponent value has been predicted to be $\tau' = 1.527$ [6]. For our five realizations of the 400×2500 IPwt, we have determined the avalanches which occur after 1% of the porous medium has been invaded. Fig. 8 shows the number, $N \geqslant 1$, of avalanches of each possible mass from one up to the largest size. Not surprisingly, there is significant noise in the small numbers of the largest masses.

The dashed line in Fig. 8 shows the predicted power law, Eq. (5). Clearly, this data is consistent with a slightly smaller value of the exponent; best fits are consistent with an exponent $\tau' = 1.37$ (shown by the solid line). As will be discussed in a following section, we believe that this 'depinning' system [13] has not achieved the self-organized critical point, after just 1% invasion, so that Fig. 8 does not show the asymptotic scaling behavior. As expected, including only later avalanches gives a somewhat improved value of the exponent.

The correlations between invaded sites show the expected scaling behavior, with exponents which, again, may not be asymptotic [6]. These correlations, $N(r,T)$, describe

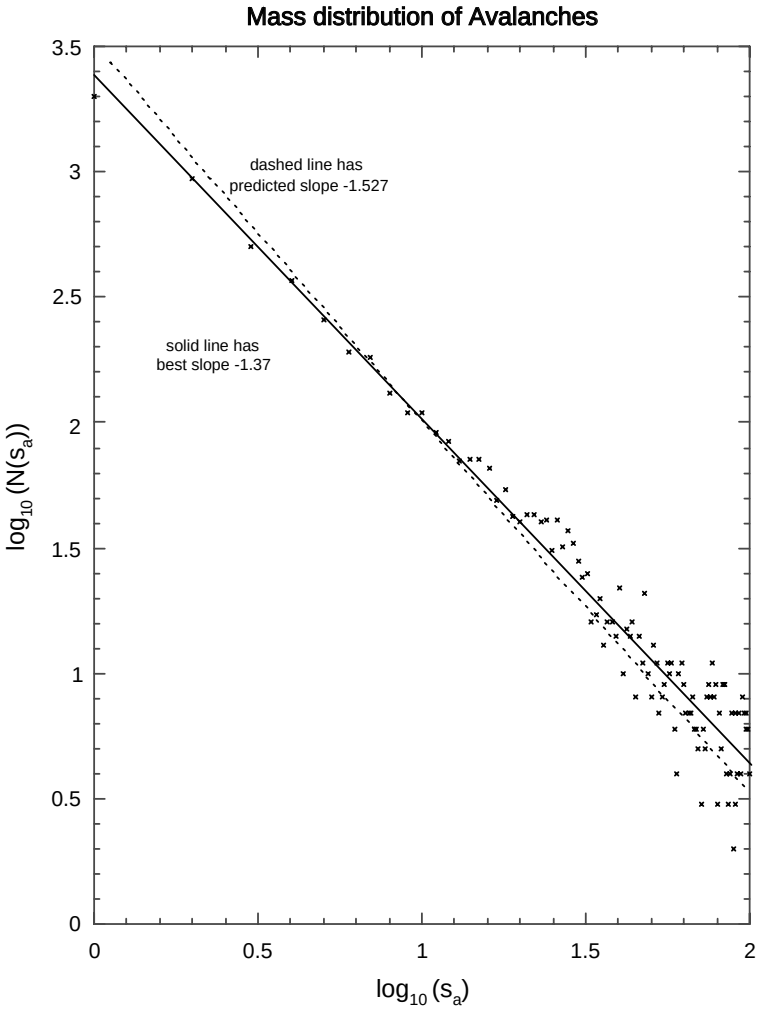

Fig. 8. The mass distribution of avalanches from our five realization of IPwt on our 400×2500 diamond lattice system. The figure only shows those avalanches which occur after 1% of the porous medium has been invaded.

the space–time correlation of any invaded site (the 'initial' site) to subsequently invaded sites. Specifically, $N(r, T)$ is the number of sites invaded, which are a distance $r \pm 0.5$ from the 'initial' site, and which are invaded T time steps after the 'initial' site was. These correlations are shown in Fig. 9 for several times. These correlations were observed [7] to scale as

$$N(r,t) = f(r^D/t)/r\,, \tag{6}$$

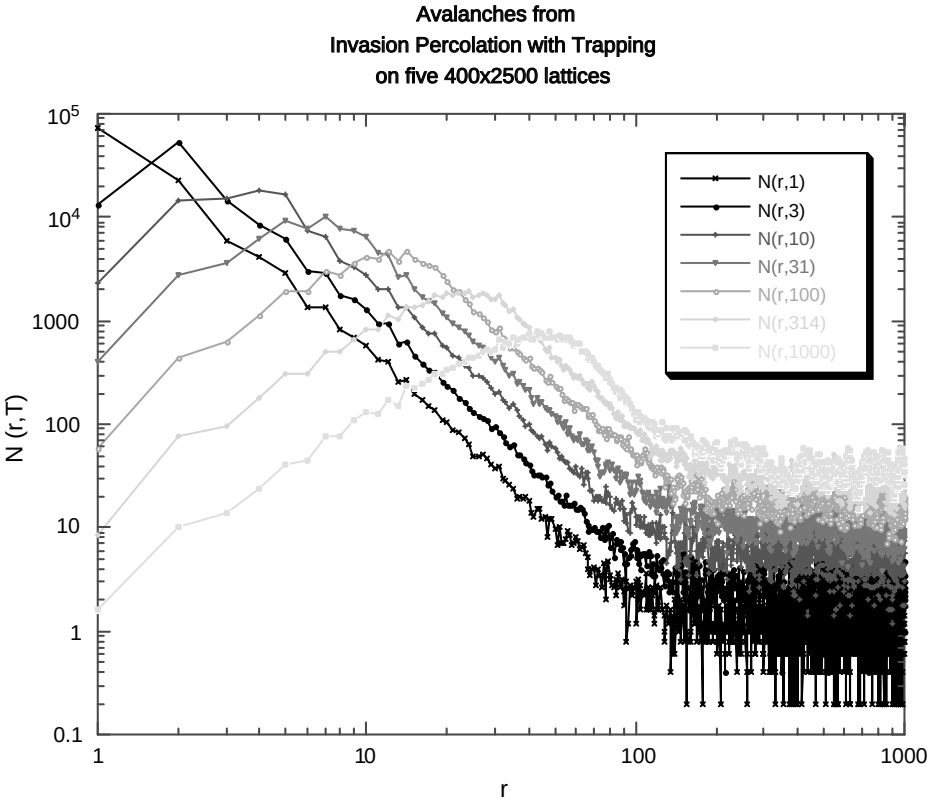

Fig. 9. Correlations, $N(r,T)$, describe the space–time correlation of any invaded site (the 'initial' site) to subsequently invaded sites. Specifically, $N(r,T)$ is the number of sites invaded, which are a distance $r \pm 0.5$ from the 'initial' site, and which are invaded T time steps after the 'initial' site was invaded. Only sites which were invaded after 1% of the 400×2500 porous medium was occupied are included.

where the scaling function had power-law asymptotic behavior

$$f(u) \approx u^{a} \quad \text{for } u \ll 1 \text{ and } f(u) \approx u^{-b} \text{ for } u \gg 1 \,. \tag{7}$$

Having used a value of fractal dimension, $D = 1.82$, the exponent values in Eq. (7) were observed to have the values $a \approx 1.4$ and $b \approx 0.6$ [7]. Scaling arguments for these exponents predict $b = 0.527$ and $a = 1.0$ [6]. Using the fractal dimension from percolation theory, $D = 1.89$ [15], we find a satisfactory scaling collapse of the data in Fig. 9 to one universal curve, shown in Fig. 10. The value of both exponents from the data in Fig. 10 are about 10% larger than the earlier estimates [7]. Since, as will be argued, our systems are not at the asymptotic self-organized critical point, it seems likely that we should not expect correct asymptotic critical values of these exponents.

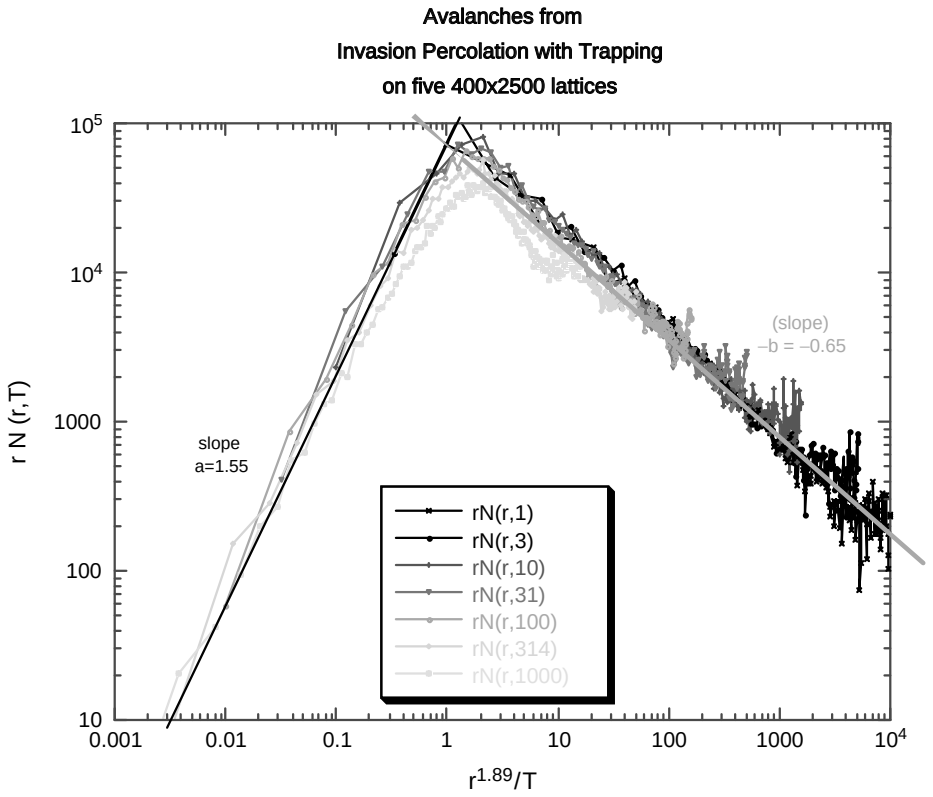

Fig. 10. Scaling collapse of the correlation function data in Fig. 9 using the percolation theory value of the fractal dimension, $D = 1.89$.

5. Spatial distribution of the avalanches

In studying results from our one million site IPwt model, we have characterized those avalanches that occurred between 1% of the occupation of the medium and breakthrough. We found results consistent with earlier work for the space–time correlation. However, there were small discrepancies between the best exponent values from our results and the previously determined exponents. Also, although the presence of avalanches explains the noise in our fractional flow profiles (Figs. 5 and 6), the fingering and the related small values of saturation of the injected fluid are not explained simply by the existence of avalanches. In this section, we will show (i) that our systems have not achieved a self-organized critical point, so that our values of the exponents should differ slightly from the asymptotic values, and (ii) that the size of the average avalanche increases with distance from the inlet. Therefore, it is more likely that large avalanches will occur at the ends of long fingers than at the ends of short fingers resulting in preferential growth of the longer fingers.

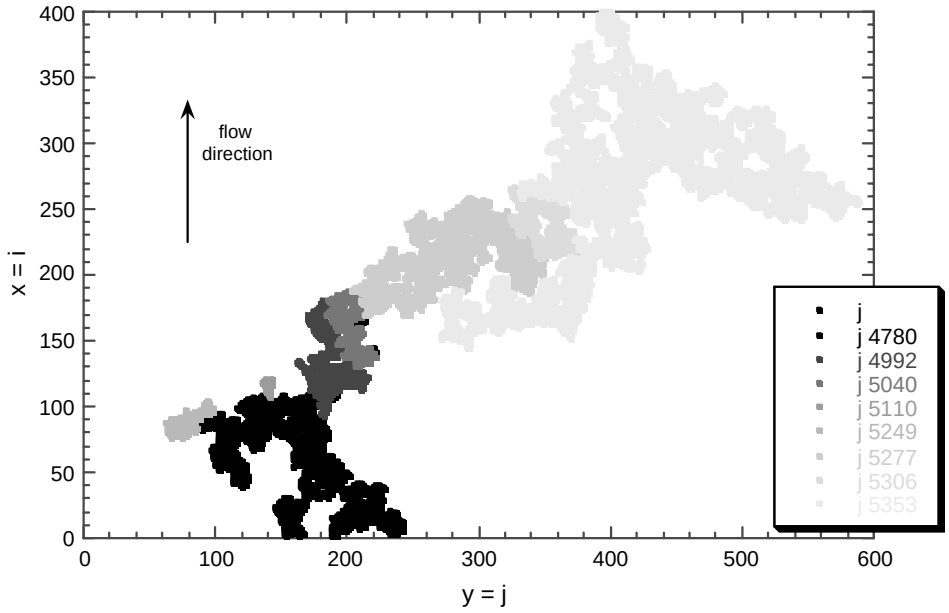

Fig. 11. The avalanche structure of the breakthrough finger for one of the realizations of our 400×2500 IPwt systems. Note the lightest gray is for the final 'breakthrough' avalanche (the 5353rd avalanche). The black squares are for all of the smallest avalanches; although a few of these smallest avalanches occur around $i = 150$, most of the smallest avalanches occur for $i < 100$.

As a precursor to studying the spatial avalanche structure of the fingers, Fig. 11 shows the avalanche structure of a typical breakthrough finger (reaching the outlet at $x{=}i{=}401$). The different gray scale areas represent different avalanches (with sequential avalanche labels 4780, 4992, 5440, ..., 5353). All of the very smallest avalanches are labeled by dark squares.

It is striking that the largest avalanche is the breakthrough avalanche. To demonstrate that it is not unusual for the largest avalanches to occur farthest from the inlet, Fig. 12 shows the avalanche size vs. $i_{\max}$, the location of the that point in the avalanche which is furthest from the inlet (therefore breakthrough avalanches should occur at $i_{\max} = 401$). It is clear that the majority of small avalanches occur near the inlet, and that the range of avalanche sizes increases with $i_{\max}$. There is a definite cutoff, $\text{Mass}_{\max}(i_{\max})$, for this data, i.e., no avalanche sizes greater than this cutoff, $\text{Mass}_{\max}(i_{\max})$, occur for a given $i_{\max}$. The cutoff shows that at a given $i_{\max}$ (say $i_{\max} = 100$) there are no avalanches greater than $\text{Mass}_{\max}(i_{\max})$ ($\text{Mass}_{\max}(i_{\max} = 100) \approx 2500$). It is well known that at a self-organized critical point, one has avalanches of all sizes obeying a power-law distribution; this cutoff demonstrates that the system is not yet critical so that any exponents determined from this data will only approximate their true asymptotic values.

These results also suggest that the average avalanche size will increase as x increases (as the self-organized critical point is approached). To investigate this possibility, we

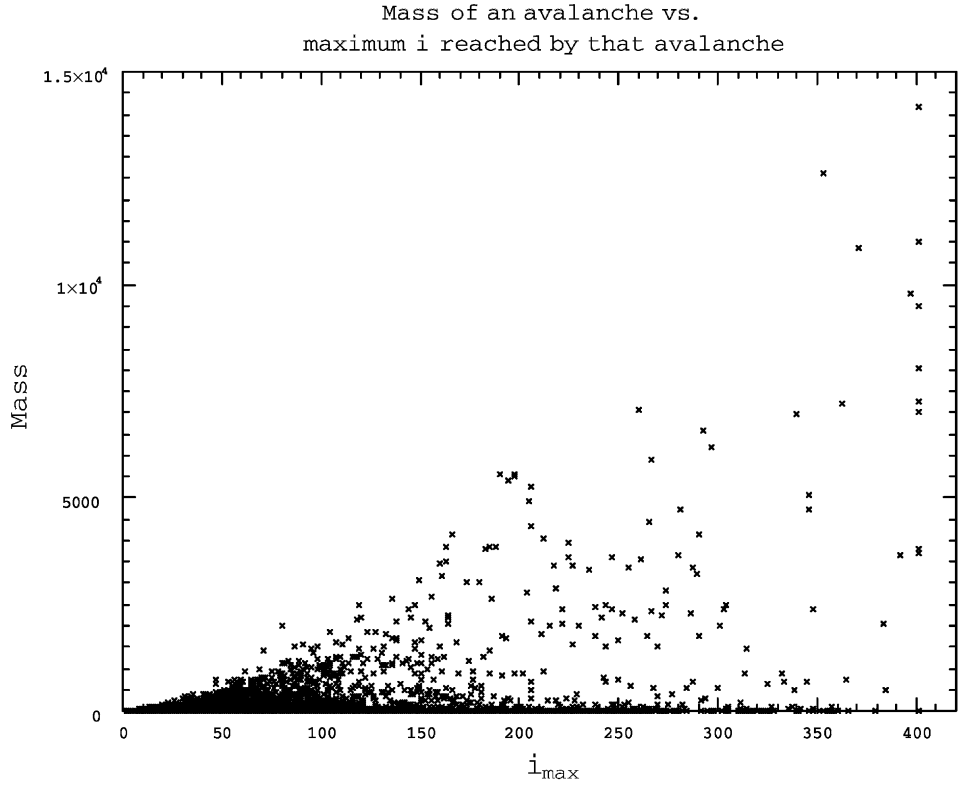

Fig. 12. For the nine realizations of our million site IPwt model, the size of each avalanche is plotted vs. the maximum distance from the inlet reached by that avalanche. Notice, of the nine breakthrough avalanches (for which $i_{\max} = 401$) four of them are among the seven largest avalanches.

determined the position of the center of mass of each avalanche. After binning the x component of the center of mass (e.g. for bins of size 1, individual bins span the range of values $x = 1$–2, 2–3, 3–4, etc.) we determined the average size of the avalanches in each of these bins. Fig. 13 shows the average avalanche size vs. bin location. Not surprisingly, there is significant noise for the bins with largest x since these have the smallest numbers of avalanches. Clearly, the average avalanche size increases with the average distance from the inlet. The power law

$$\langle s_{\mathrm{a}} \rangle \approx \langle x \rangle^{1.1} \tag{8}$$

is a credible fit to the data up to $\langle x \rangle = 100$ where the noise is too large for a reliable fit. However, a linear increase of avalanche size with distance is allowed by generous uncertainties in the exponent. In any case, the average avalanche size increases significantly with distance from the inlet.

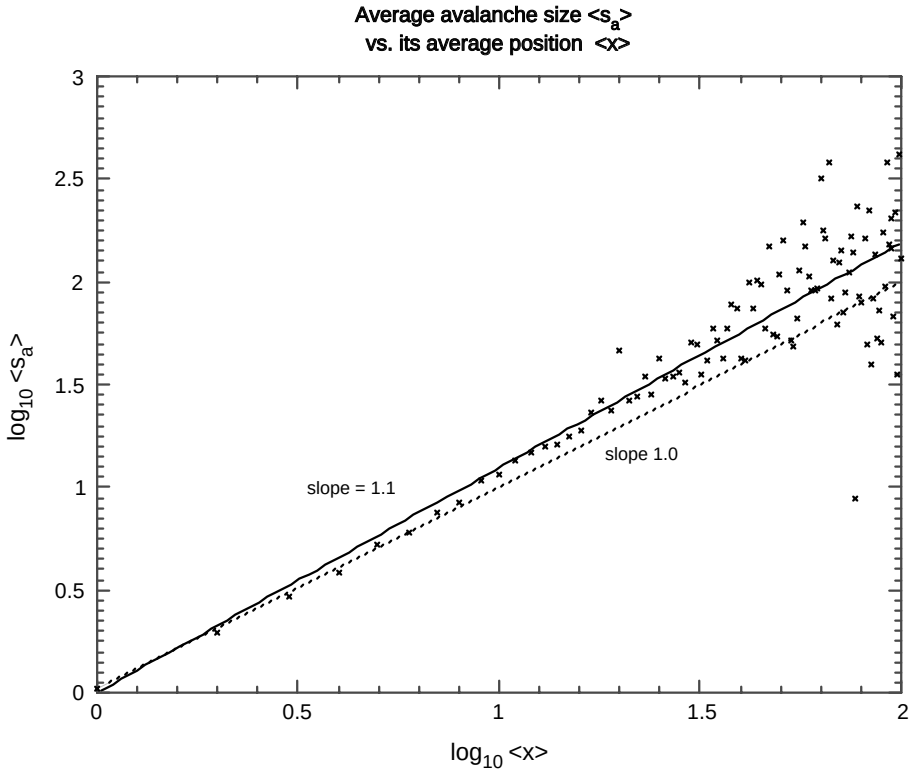

Fig. 13. Average size of the avalanches vs. their average distance from the inlet. The avalanche data has been put into bins of size 1 depending upon which bin the x component of their center of mass places them (actually the $\langle x \rangle$ of the horizontal axis is the location of the center of the bin). The solid line shows the best power law fit in Eq. (8); the dashed line shows the linear power law.

6. Conclusions

Invasion Percolation was introduced 20 years ago to describe two-phase flow in porous media in the limit where capillary effects dominate and viscous effects are negligible (zero capillary number) [2,3]. Over the past 20 years, the model was the subject of a number of investigations, but practical issues relating to the causes of low injected fluid saturation and fingering have not received concentrated attention [4–8]. In this paper, we have focused on these issues. In Section 2, we showed that the average position of the injected fluid has the standard fractal-scaling behavior, consistent with the fractal dimension of ordinary critical percolation [15]. Profiles of the invading fluid saturation were shown to scale with the fractal dimension, in Section 3. Earlier work on IP demonstrated the existence of avalanches (or 'bursts' or 'Haines jumps') which likely contributed to the random noise in the average position of the injected fluid, Fig. 2. Unfortunately, the random spatial and temporal occurrence of these avalanches made an average analysis of the fractional flow intractable. The fractional flow profiles

showed both significant differences between different realizations (e.g. Figs. 6a and b) and an irregular time evolution as the interface advanced through the medium (e.g. Figs. 5a and b); these irregularities even occurred in our million site systems where the profiles were averaged over the 2500 pore body width. In Section 4, it was shown that the spatial and time dependence of the correlations between invaded sites obeys the predicted scaling behavior, with exponents which differ by as much as 10% from previous work [6,7]. In Section 5, we show that these finite size systems are not yet at the self-organized critical point, so that the effective exponents determined in the previous section should not be expected to have their asymptotic critical values. These finite systems are not critical because avalanches which reach any finite value of x have a definite cut-off, Fig. 12, so that at finite x, the system does not have the critical power-law distribution with all sizes of avalanches [10,11]. In this section, it is also demonstrated that the average size of an avalanche increases with the distance of its center of mass from the inlet. Therefore, the size of a typical avalanche increases with its distance from the inlet. This favors preferential growth of long fingers over shorter fingers because the avalanches occurring at the end of long fingers will tend to be larger advancing the long finger more. We plan to perform larger simulations so that we can determine more reliable estimates of the critical indices.

Acknowledgements

M. Ferer and G. Bromhal gratefully acknowledge the support of the US Department of Energy, Office of Fossil Energy. This work was performed while Grant Bromhal held a National Research Council Associateship Award at the National Energy Technology Laboratory.

References

[1] G.L. Stegemeier, Mechanisms of entrapment and mobilization of oil in porous media, in: D.O. Shah, R.S. Schechter (Eds.), Improved Oil Recovery by Surfactant and Polymer Flooding, Academic Press, New York, 1977, p. 55.
[2] R. Chandler, et al., J. Fluid Mech. 119 (1982) 249.
[3] D. Wilkinson, J.F. Willemsen, J. Phys. A 16 (1983) 3365.
[4] J. Feder, Fractals, Plenum Press, New York, 1988.
[5] T. Vicsek, Fractal Growth Phenomena, World Scientific, Singapore, 1989.
[6] S. Roux, E. Guyon, J. Phys. A 22 (1989) 3693–3705.
[7] L. Furuberg, et al., Phys. Rev. Lett. 61 (1988) 2117–2120.
[8] P. Meakin, Fractals, Scaling, and Growth Far from Equilibrium, Cambridge University Press, Cambridge, 1998.
[9] M. Ferer, G.S. Brohmal, D.H. Smith, Ground Water Res., 2002, submitted for publication.
[10] P. Bak, C. Tang, K. Wiesenfeld, Phys. Rev. Lett. 59 (1987) 381–384.
[11] P. Bak, C. Tang, K. Wiesenfeld, Phys. Rev. A 38 (1988) 364–374.
[12] M. Ferer, et al., Phys. Rev. E 47 (1993) 2713.
[13] M. Paczuski, S. Maslov, P. Bak, Phys. Rev. E 53 (1996) 414–443.
[14] J. Nittmann, G. Daccord, H.E. Stanley, Nature 314 (1985) 141–144.
[15] D.S. Stauffer, Introduction to Percolation Theory, Taylor & Francis, Philadelphia, 1985.